Supplementary Material

Computational exploration of two-dimensional vacancy-free boridene sheet and its derivatives: High stabilities and the promise for hydrogen evolution reaction

Yuying Zhao[1,#], Jincan Zhang[1,#], Fengxian Ma[1], Hongbo Wu[1], Weizhen Meng[1], Ying Liu[1], Yalong Jiao[1], Aijun Du[2]

[1]College of Physics, Hebei Key Laboratory of Photophysics Research and Application, Hebei Normal University, Shijiazhuang 050024, Hebei, China.
[2]School of Chemistry and Physics and Centre for Materials Science, Queensland University of Technology, Gardens Point Campus, Brisbane, QLD 4000, Australia.

[#]Authors contributed equally.

Correspondence to: Prof. Fengxian Ma, College of Physics, Hebei Key Laboratory of Photophysics Research and Application, Hebei Normal University, Shijiazhuang 050024, Hebei, China. E-mail: fengxianma@hebtu.edu.cn; Prof. Yalong Jiao, College of Physics, Hebei Key Laboratory of Photophysics Research and Application, Hebei Normal University, Shijiazhuang 050024, Hebei, China. E-mail: yalong.jiao@hebtu.edu.cn

How to cite this article: Zhao Y, Zhang J, Ma F, Wu H, Meng W, Liu Y, Jiao Y, Du A. Computational exploration of two-dimensional vacancy-free boridene sheet and its derivatives: High stabilities and the promise for hydrogen evolution reaction. *Microstructures* 2024;4:xx. http://dx.doi.org/10.20517/microstructures.2023.80

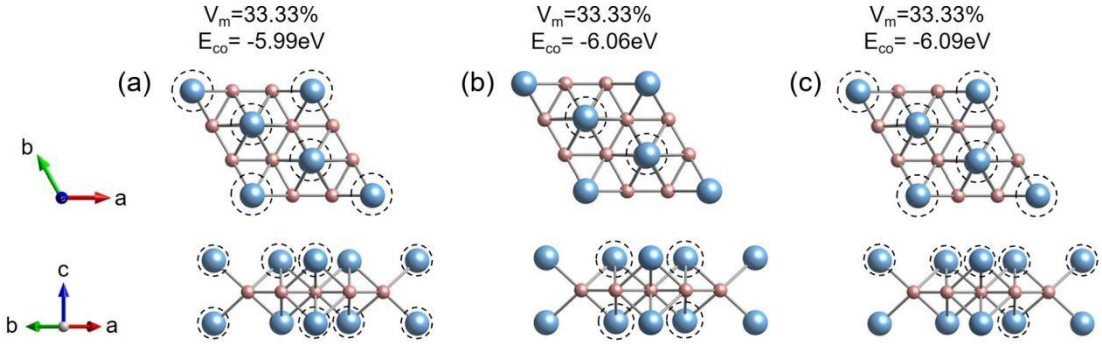

Figure S1. (a-c) Top view and side view of the Mo_2B_6 structure with three different vacancy distributions. Dashed circles represent the vacancy sites. The vacancy concentration (V_m) and cohesive energy (E_{co}) of each configuration are also indicated.

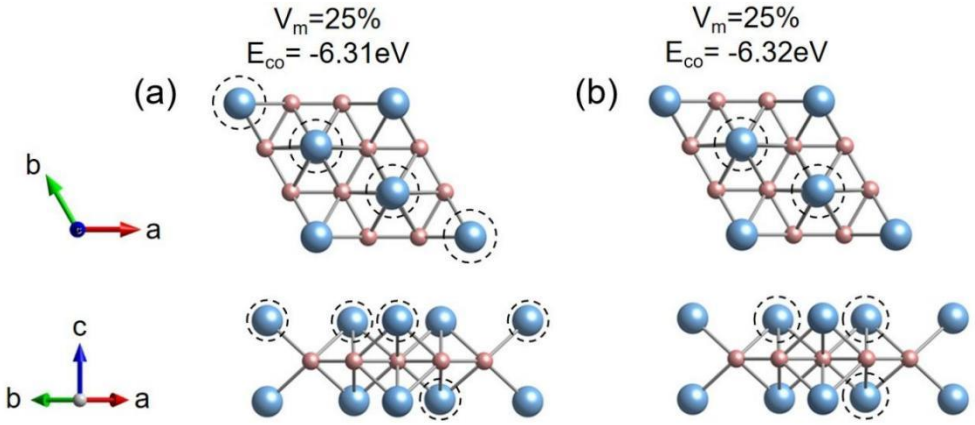

Figure S2. (a-b) Top view and side view of the Mo_3B_6 structure with two different vacancy distributions. Dashed circles represent the vacancy sites. The vacancy concentration (V_m) and cohesive energy (E_{co}) of each configuration are also indicated.

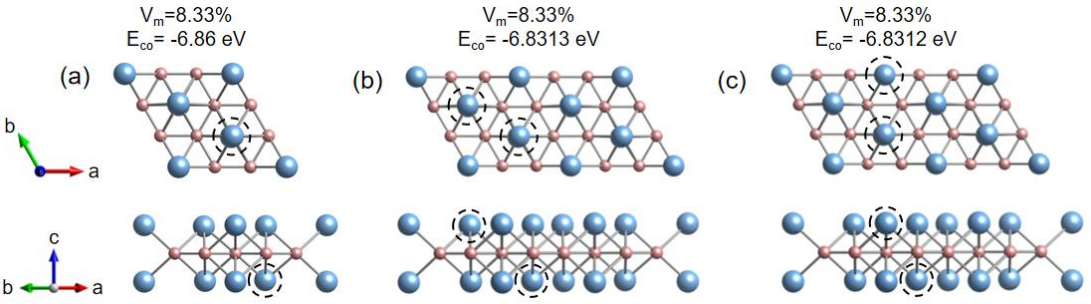

Figure S3. Vacancy distributions of (a) Mo_5B_6, and (b-c) $Mo_{10}B_{12}$ sheets. Dashed circles represent the vacancy sites. The vacancy concentration (V_m) and cohesive energy (E_{co}) of each configuration are also indicated.

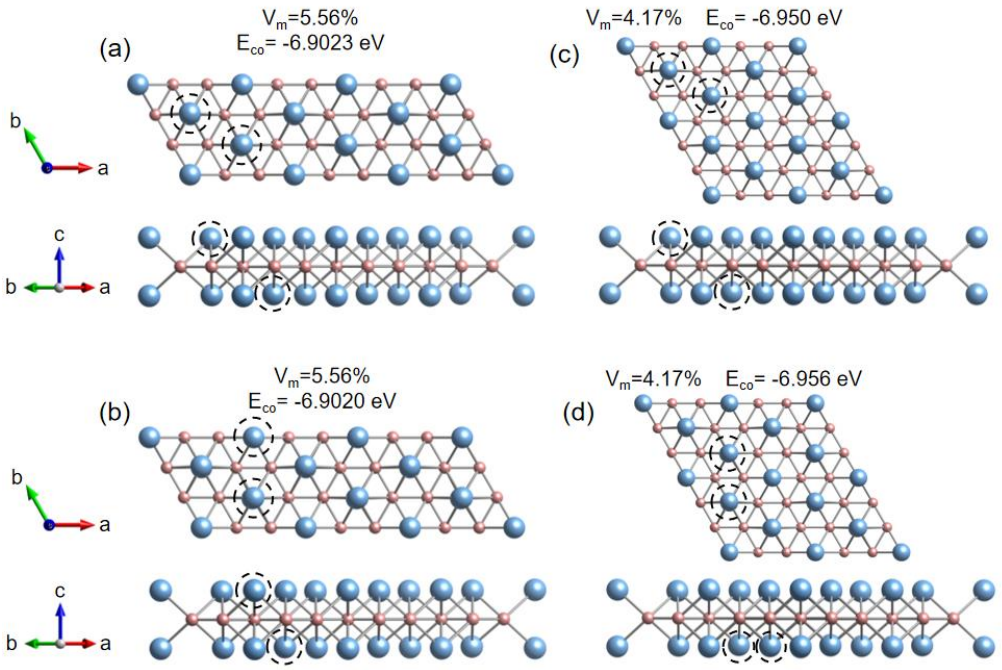

Figure S4. Vacancy distributions of (a-b) $Mo_{16}B_{18}$, and (c-d) $Mo_{22}B_{24}$ sheets. Dashed circles represent the vacancy sites. The vacancy concentration (V_m) and cohesive energy (E_{co}) of each configuration are also indicated.

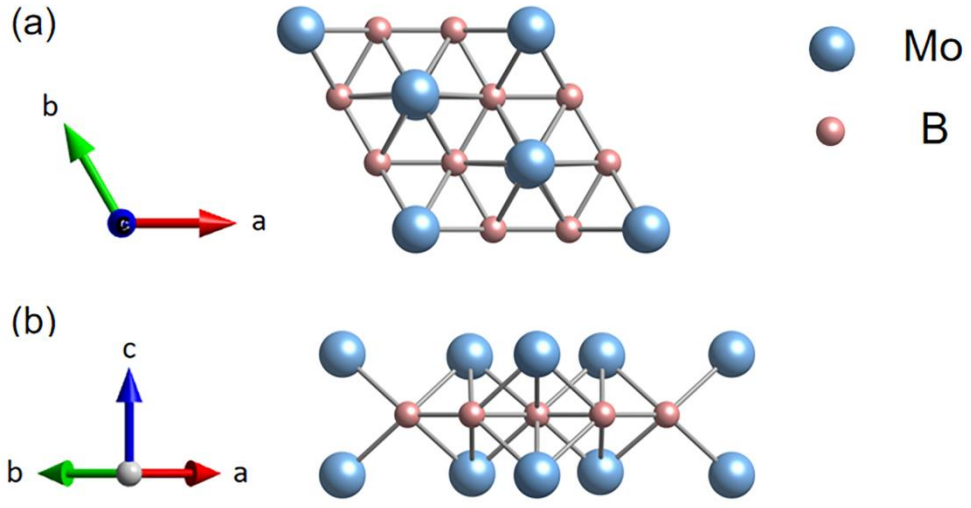

Figure S5. Top view and side view of the Mo_6B_6 structure.

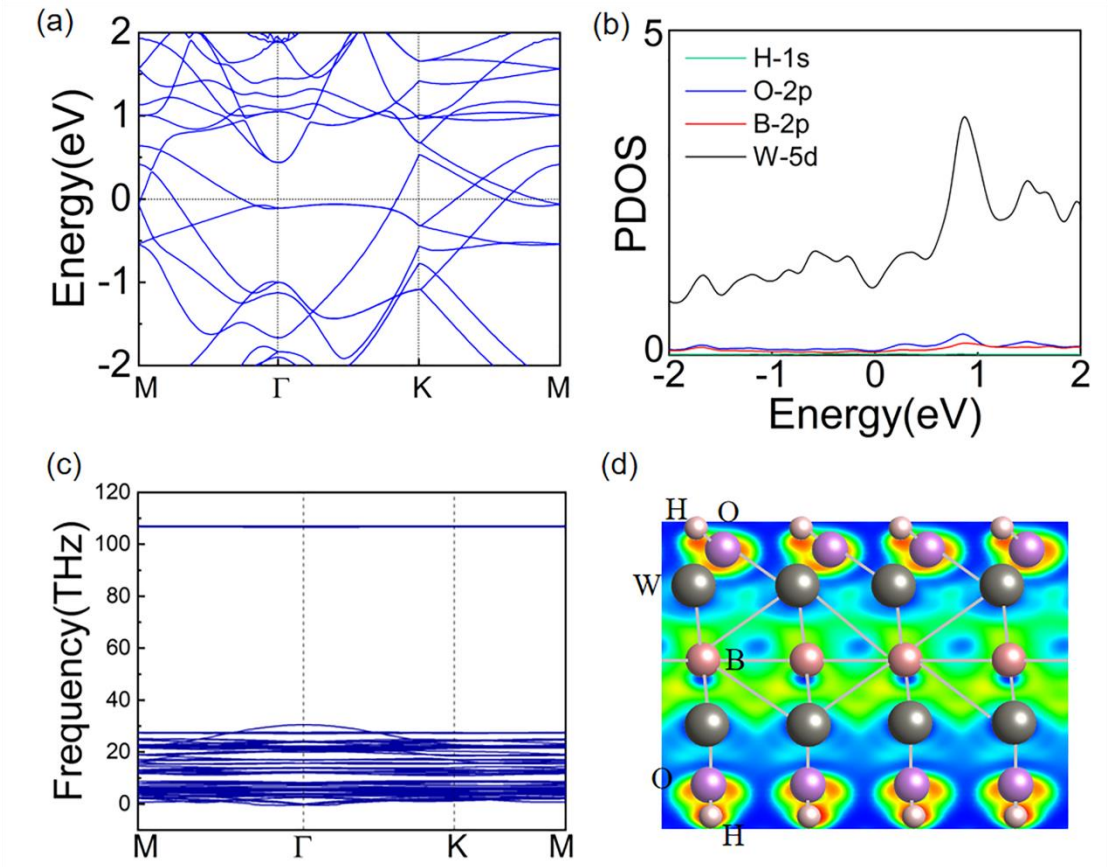

Figure S6. (a) Band structure, (b) partial density of states, (c) phonon spectrum and (d) ELF along (001) plane for the $W_6B_6(OH)_6$ sheet.

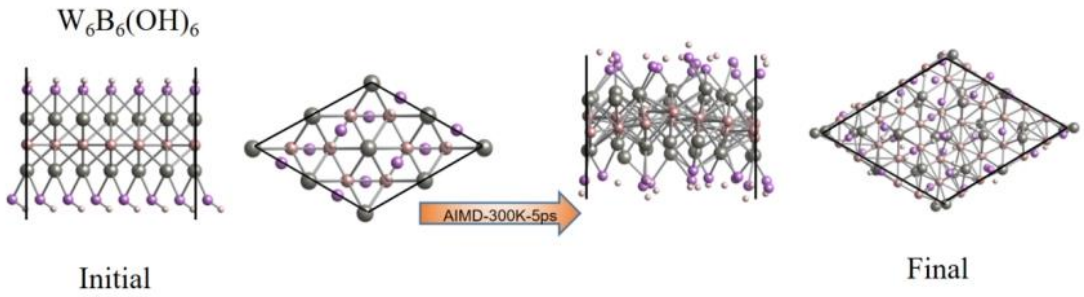

Figure S7. AIMD simulated results of $W_6B_6(OH)_6$ at 300 K for 5 ps. The initial and final structures (side and top views) are shown for illustrations.

In our study, we found that the $W_6B_6(OH)_6$ sheet displays dynamic stability as evident from Fig. S6c. However, through the implementation of AIMD simulation captured in Fig. S7, it became apparent that the structure of the sheet fails. Consequently, we have chosen to exclude its discussion from the main text.

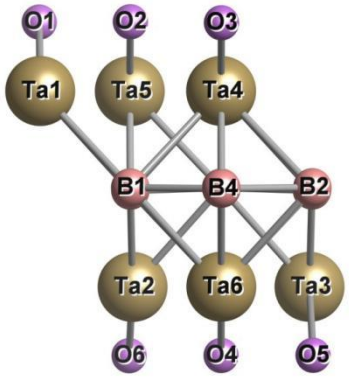

atom	charge transfer
Ta1	+2.09e
Ta2	+1.64e
Ta3	+2.00e
Ta4	+2.19e
Ta5	+1.41e
Ta6	+2.33e
O1	-1.38e
O2	-1.38e
O3	-1.18e
O4	-1.32e
O5	-1.28e
O6	-1.42e

Figure S8. Bader charge analysis for the $Ta_6B_6O_6$ sheet.

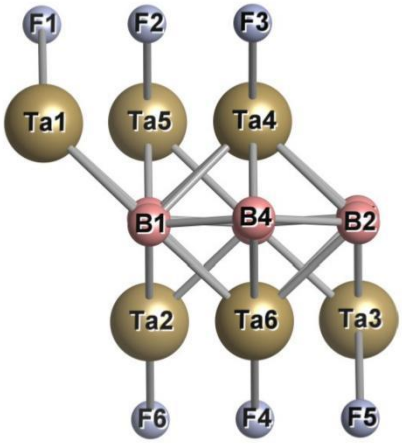

atom	charge transfer
Ta1	+1.86e
Ta2	+1.55e
Ta3	+1.50e
Ta4	+1.90e
Ta5	+1.83e
Ta6	+1.57e
F1	-1.04e
F2	-1.02e
F3	-1.03e
F4	-0.91e
F5	-0.93e
F6	-0.93e

Figure S9. Bader charge analysis for the $Ta_6B_6F_6$ sheet.

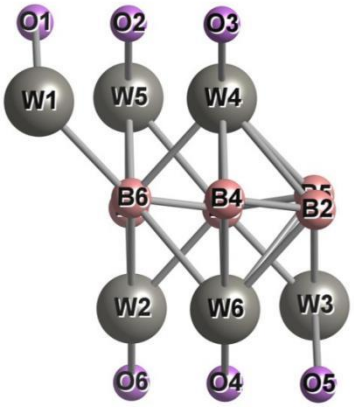

atom	charge transfer
W1	+1.98e
W2	+1.99e
W3	+1.96e
W4	+1.99e
W5	+2.00e
W6	+1.99e
O1	-1.24e
O2	-1.24e
O3	-1.24e
O4	-1.20e
O5	-1.20e
O6	-1.19e

Figure S10. Bader charge analysis for the $W_6B_6O_6$ sheet.

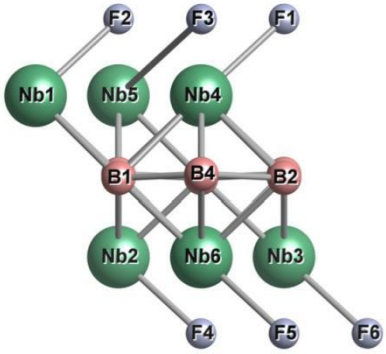

atom	charge transfer
Nb1	+1.66e
Nb2	+1.54e
Nb3	+1.51e
Nb4	+1.67e
Nb5	+1.66e
Nb6	+1.53e
F1	-0.93e
F2	-0.93e
F3	-0.92e
F4	-0.87e
F5	-0.88e
F6	-0.87e

Figure S11. Bader charge analysis for the $Nb_6B_6F_6$ sheet.

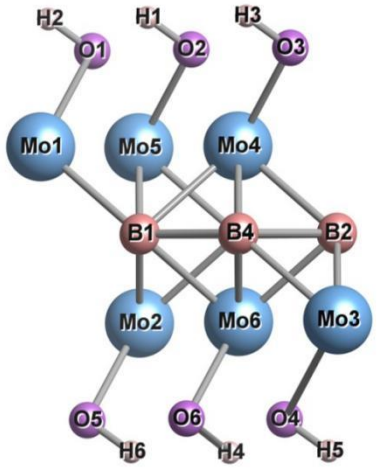

atom	charge transfer
Mo1	+1.54e
Mo2	+1.53e
Mo3	+1.53e
Mo4	+1.54e
Mo5	+1.54e
Mo6	+1.53e
O1	-0.24e
O2	-0.23e
O3	-0.24e
O4	-0.24e
O5	-0.23e
O6	-0.24e
H1	-0.53e
H2	-0.53e
H3	-0.53e
H4	-0.52e
H5	-0.52e
H6	-0.53e

Figure S12. Bader charge analysis for the $Mo_6B_6(OH)_6$ sheet.

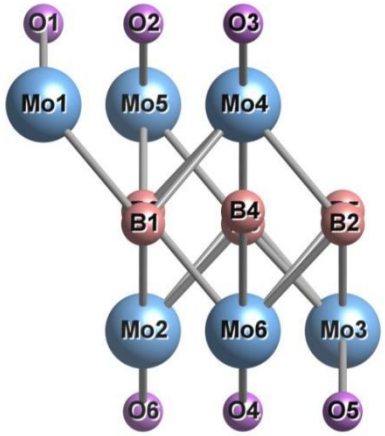

atom	charge transfer
Mo1	+1.75e
Mo2	+1.72e
Mo3	+1.72e
Mo4	+1.75e
Mo5	+1.75e
Mo6	+1.72e
O1	-1.10e
O2	-1.10e
O3	-1.10e
O4	-1.07e
O5	-1.07e
O6	-1.07e

Figure S13. Bader charge analysis for the $Mo_6B_6O_6$ sheet.

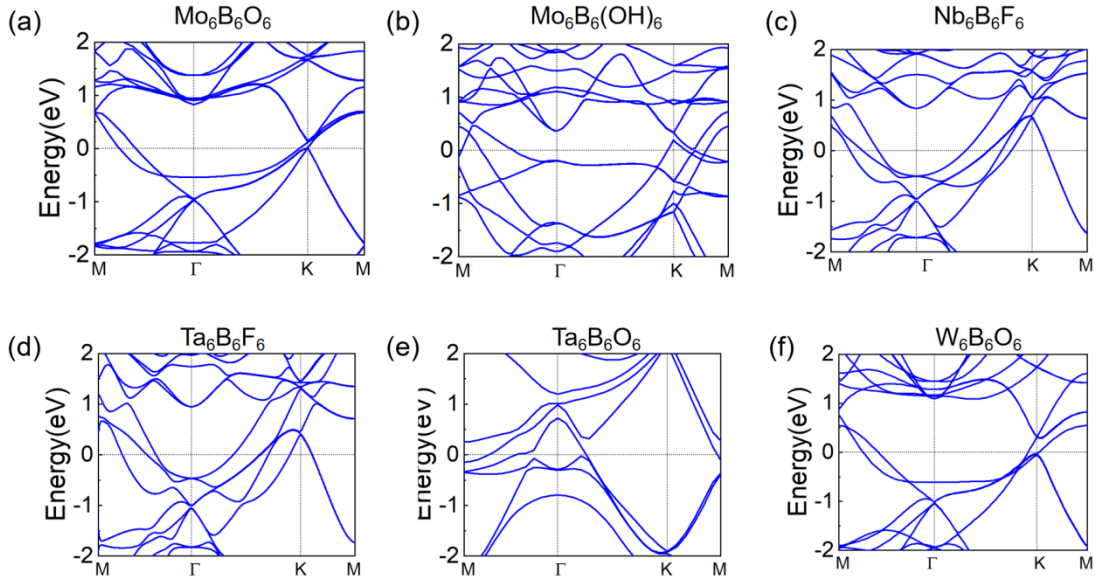

Figure S14. Band structures for different $M_6B_6T_6$ sheets on HSE06 level.

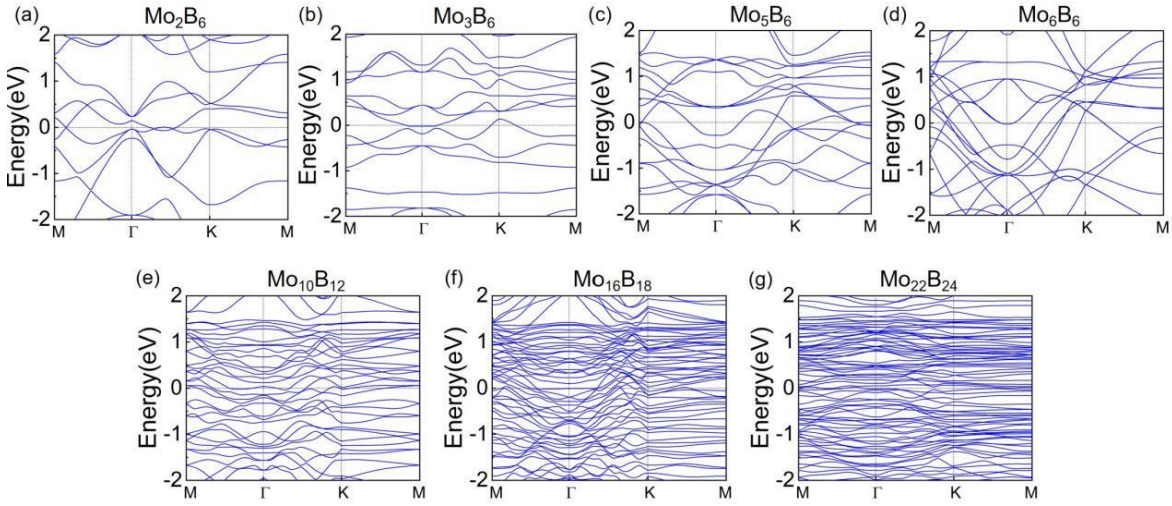

Figure S15. Band structures for different Mo_xB_y sheets on PBE level.

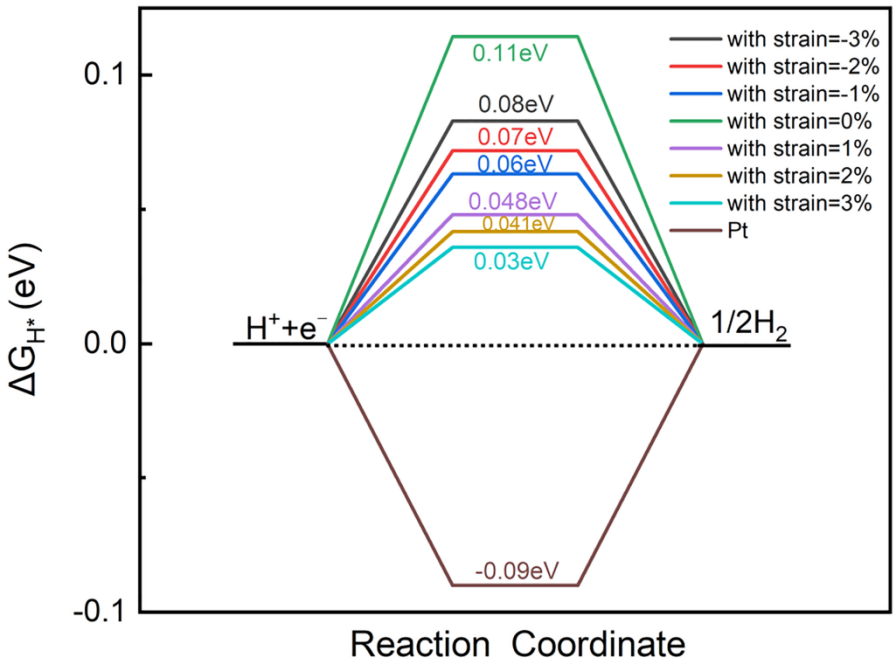

Figure S16. Gibbs free energy (ΔG_H*) at the O sites of the $Mo_6B_6(OH)_6$ monolayer under different strains(ε).

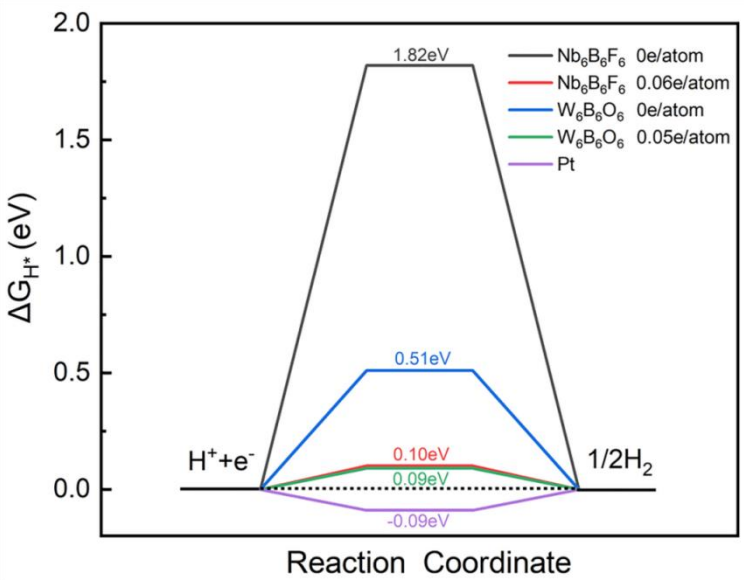

Figure S17. Gibbs free energy (ΔG_H*) for $Nb_6B_6F_6$ and $W_6B_6O_6$ sheet under neutral or charged states.

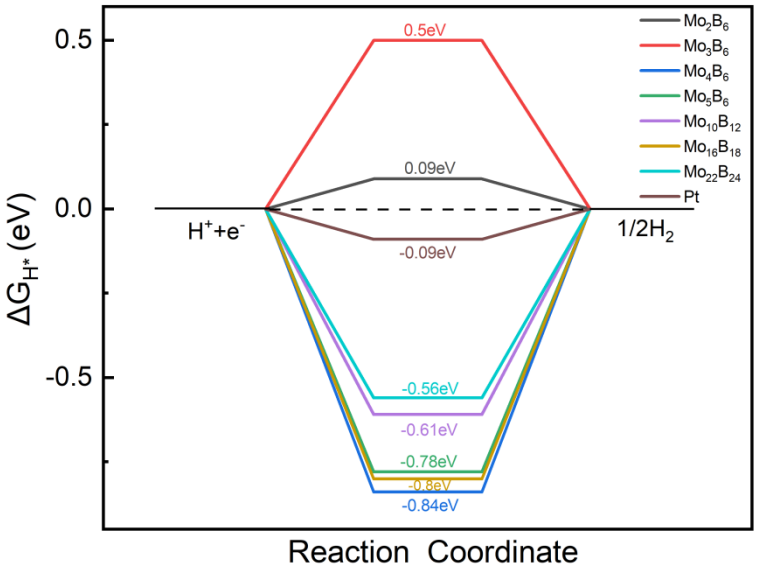

Figure S18. Gibbs free energy (ΔG_H*) for Mo_xB_y sheets with different vacancy concentrations.

Table S1. Lattice constants (in Å), cohesive energies (in eV), elastic constants (N/m), Poisson's ratio ν, and Young's modulus (in GPa·nm) for the $W_6B_6(OH)_6$ sheet.

System	a	b	Cohesive Energy	C_{11}	C_{22}	C_{12}	C_{44}	ν	Young's modules
$W_6B_6(OH)_6$	5.50	5.24	-5.98	191.18	242.39	54.71	76.80	0.29	226.73

Table S2. The elastic constants (N/m), Poisson's ratio ν, and Young's modulus (in GPa·nm) for the Mo_xB_y sheets.

System	C_{11}	C_{22}	C_{12}	C_{44}	ν	Young's modules
Mo_2B_6	111.76	111.47	15.53	46.16	0.14	109.60
Mo_3B_6	155.19	155.69	38.15	58.54	0.25	144.12
Mo_4B_6	115.02	115.32	39.78	36.96	0.35	101.57
Mo_5B_6	219.98	218.59	54.85	82.10	0.25	206.21
Mo_6B_6	236.87	239.82	43.34	97.72	0.18	231.90
$Mo_{10}B_{12}$	177.17	190.06	36.54	72.80	0.21	182.51
$Mo_{16}B_{18}$	200.20	207.66	46.20	77.13	0.23	196.99
$Mo_{22}B_{24}$	208.14	209.84	46.64	80.54	0.22	199.39

The structure file (POSCAR) for the Mo_6B_6 sheet

Mo_6B_6

1.0

5.3826999664	0.0000000000	0.0000000000
-2.6913499832	4.6615549119	0.0000000000
0.0000000000	0.0000000000	22.3838996887

Mo B

6 6

Direct

0.000000000	0.000000000	0.564570010
0.333330005	0.666670024	0.437169999
0.000000000	0.000000000	0.435429990
0.666670024	0.333330005	0.562829971
0.338310003	0.684140027	0.562049985
0.648469985	0.322970003	0.438919991
0.335139990	0.000000000	0.500000000
0.000000000	0.335139990	0.500000000
0.664860010	0.664860010	0.500000000
0.664860010	0.000000000	0.500000000
0.000000000	0.664860010	0.500000000
0.335139990	0.335139990	0.500000000